

Understanding the High Solubility of CO₂ in an Ionic Liquid with the Tetracyanoborate Anion

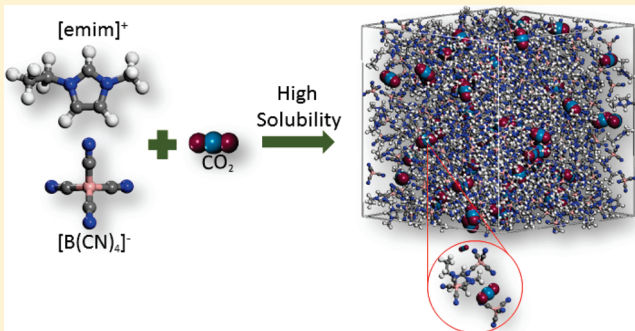
Ravichandar Babarao,[†] Sheng Dai,^{†,‡} and De-en Jiang^{*,†}

[†]Chemical Science Division, Oak Ridge National Laboratory, Oak Ridge, Tennessee 37831, United States

[‡]Department of Chemistry, University of Tennessee, Knoxville, Tennessee 37966, United States

 Supporting Information

ABSTRACT: The ionic liquid 1-ethyl-3-methylimidazolium tetracyanoborate, [emim][B(CN)₄], shows greater CO₂ solubility than several popular ionic liquids (ILs) of different anions including [emim]bis(trifluoromethylsulfonyl)imide [emim][Tf₂N]. Herein, both classical molecular dynamics simulation and quantum mechanical calculations were used to understand the high solubility of CO₂ in the [emim][B(CN)₄] IL. We found that the solubility is dictated by the cation–anion interaction, while the CO₂–anion interaction plays a secondary role. The atom–atom radial distribution functions (RDFs) between cation and anion show weaker interaction in [emim][B(CN)₄] than in [emim][Tf₂N]. A good correlation is observed between gas-phase cation–anion interaction energy with CO₂ solubility at 1 bar and 298 K, suggesting that weaker cation–anion interaction leads to higher CO₂ solubility. MD simulation of CO₂ in the ILs showed that CO₂ is closer to the anion than to the cation and that it interacts more strongly with [B(CN)₄] than with [Tf₂N]. Moreover, a higher volume expansion is observed in [emim][B(CN)₄] than in [emim][Tf₂N] at different mole fractions of CO₂. These results indicate that [B(CN)₄] as a small and highly symmetric anion is unique in giving a high CO₂ solubility by interacting weakly with the cation and thus allowing easy creation of cavity for close contact with CO₂.



1. INTRODUCTION

Separation of gas mixtures, particularly CO₂ from other gases, remains a major interest of research due to its implication on global warming. In order to replace the more energy-intensive processes such as amine scrubbing for CO₂ separation with more energy-efficient methods, several alternative technologies have been explored. One such process is membrane separation which is steadily growing since its introduction.¹ Room temperature ionic liquids (RTILs) with their nonflammability, negligible vapor pressure, and high thermal stability have been used to separate gas mixtures in supported liquid membranes; several reviews have discussed the importance of RTILs for gas separation including the solubility and permeability of gases for membrane applications.^{2–5}

A membrane's permeability for a specific gas is the product of its solubility and diffusivity. So high solubility can lead to high permeability and selectivity, and it is of great interest to find ionic liquids with greater CO₂ solubility and at the same time lower or not significantly higher viscosity. CO₂ solubility in many ionic liquids has been measured for different temperatures and pressures.⁷ Solubility in an IL can be based on per unit mole, weight, or volume of the ionic liquid. We agree with some researchers that the per-volume basis is more useful for engineering design.² Although it is simple to use, the mole-fraction unit can be greatly biased for an IL with great molecular weight. So here we use the per-volume

solubility when comparing CO₂ solubility among different ILs. CO₂ solubility observed in ionic liquids ranges from 1.44 to 2.44 cm³(STP) cm⁻³ atm⁻¹ for the temperature window of 298–313 K.²

1-Alkyl-3-methylimidazolium bis(trifluoromethylsulfonyl)imide ILs show some of the highest CO₂ solubility among the ILs.^{8,9} Changing or modifying either cation or anion has been employed to improve the CO₂ solubility.^{10–12} For example, changing the anion from BF₄ to Tf₂N in the case of 1-ethyl-3-methylimidazolium cation increases the CO₂ solubility from 1.83 to 2.40 cm³-(STP) cm³ atm⁻¹, corresponding to an increase of 31%.² Several thermodynamic models have been developed to predict the thermodynamic and physical properties of ILs, including CO₂ solubility and diffusivity.^{13,14} COSMO-RS, a theoretical tool based on quantum chemistry calculation and continuum solvation model, has been used to predict CO₂ solubility in a wide variety of ILs.^{15,16}

In addition to experimental and theoretical models, atomistic simulations were used to explain the structural and dynamic properties of pure ILs and its mixtures. Atomistic simulations of

Received: June 9, 2011

Revised: June 29, 2011

Published: July 01, 2011

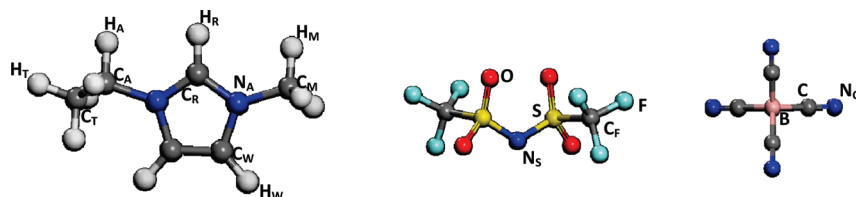


Figure 1. Schematic representation of 1-ethyl-3-methylimidazolium [emim] cation (left) bis(trifluoromethylsulfonyl)imide [Tf₂N] anion (middle) and tetracyanoborate [B(CN)₄] anion (right).

CO₂–IL mixtures have been reported by several authors and focused mainly on hexafluoroprophosphate [PF₆⁻] and bis(trifluoromethylsulfonyl)imide [Tf₂N]⁻ anions, paired with different cations.^{17–20} The importance and current status of molecular simulations of ILs have been highlighted recently in several reviews.^{21,22} Moreover, including polarization has a pronounced effect on the dynamic properties of an IL, leading to good agreement with the experiments, but less effect on the structural properties.^{23–26} The solubility behavior of CO₂ in different ILs is explained based on atomistic simulations. In this regard, Zhang et al. recently explored the mechanism of CO₂ absorption in the ionic liquid 1-*n*-hexyl-3-methylimidazolium tris(pentafluoroethyl)trifluorophosphate [hmim][FEP] using molecular simulation and mentioned that the increase in CO₂ solubility in [hmim][FEP] when compared to [hmim][PF₆⁻] is related to asymmetry of anion [FEP]⁻, more free volume, and a cooperative attraction between cation and anion.²⁰

More recently, a series of ionic liquids with nitrile-containing anions paired with 1-alkyl-3-methylimidazolium cation was tested for permeability ratio of CO₂ versus N₂ in a supported liquid membrane setup. It was found that the 1-ethyl-3-methylimidazolium tetracyanoborate [emim][B(CN)₄] IL shows rather high CO₂ solubility and CO₂/N₂ selectivity.⁶ The CO₂ solubility in [emim][B(CN)₄] is ~30% greater than the popular ionic liquid [emim][Tf₂N]. The high CO₂ solubility in [emim][B(CN)₄] is rather surprising for a small and highly symmetric anion such as [B(CN)₄]⁻ and may lead to a new class of ILs promising for CO₂/N₂ membrane separation. The main aim of this work is to understand why CO₂ solubility is high in [emim][B(CN)₄] in comparison with [emim][Tf₂N] and other ILs by using molecular dynamics simulation and quantum mechanical calculations. The models and simulation methodology are discussed briefly in section 2, followed by the results and discussion in section 3. Finally, the concluding remarks are summarized in section 4.

2. MODELS AND METHODOLOGY

MD simulations have been carried out on ILs with and without CO₂ using the DL_POLY package.²⁷ The dispersion interactions were evaluated using a cutoff of 15 Å, and a very efficient full electrostatics algorithm based on the particle mesh Ewald (PME) method was used to deal with the full electrostatic interactions. To speed up the MD simulation, a multiple time step algorithm was used. The trajectories were integrated using velocity Verlet algorithm with an initial time step of 2 fs. The temperature and pressure were controlled by the Nosé–Hoover method with a relaxation time of 0.8 and 1 ps, respectively. Statistical uncertainties in the thermodynamic properties reported in this work were calculated based on block average analysis.

All-atom force fields for ILs were used. Bonded and nonbonded parameters were from Koddemann et al.²⁸ for [emim][Tf₂N]

and from Borodin²³ for [emim][B(CN)₄] with no polarization effect included. The force-field parameters for [emim][BF₄⁻] were from Liu et al.²⁹ The Lennard-Jones parameters, partial charges, and C–O bond length of CO₂ were from the three-site EPM2 model with rigid linear geometry.³⁰ The IL structures and the labels of the atoms used in the force fields are displayed in Figure 1.

The initial configurations for MD simulations were generated by randomly distributing 256 ion pairs in a very large simulation cell using PACKMOL program.³¹ Each configuration was then energetically minimized using a zero temperature MD simulation, followed by a short NPT run at 500 K and 1000 atm to provide densely packed, mixed initial configurations. Finally, these configurations were left to relax at 1 atm and 298 K for another 2 ns until the appropriate density was achieved. For ILs with CO₂, the same procedure was employed to construct the initial configurations for different mole fractions of CO₂. NPT simulation was performed for each system at room temperature, and the corresponding pressure was set at the experimental values. The cell volume and the system energy were found to fluctuate around a mean value over the time duration, indicating that the system reached equilibration.

The gas-phase interaction energies (E_{int}) for the [emim] cation and CO₂ with different anions were calculated at the RI-MP2 level of theory in the TURBOMOLE V5.10 package using triple- ζ valence basis set with polarization (TZVPP).³² For each ion pair, different initial conformers were chosen in such a way that the more positive atom of the cation is kept close to the more negative atom of the anion and then each conformer was geometrically optimized at the MP2 level. Finally, the MP2 energies based on the most stable conformer for each ion pair and CO₂–anion were calculated.

3. RESULTS AND DISCUSSION

In this section, we first show the structural correlation based on radial distribution functions for pure [emim][Tf₂N] and [emim][B(CN)₄] ILs. Then we will discuss IL–CO₂ mixtures. Next, we demonstrate the correlation between gas-phase cation–anion interaction energies and CO₂ solubilities in ILs. Finally, the volume expansions of the [emim][Tf₂N] and [emim][B(CN)₄] ILs are compared for varying mole fractions of CO₂.

3.1. Structure of Pure ILs. We first benchmark the force fields used for the ILs in this paper, though they have been validated earlier.^{23,28,33} From constant-pressure MD simulations, we calculated the density of both ionic liquids and compared with the experiment.⁶ The density of [emim][Tf₂N] was calculated as 1.521 g/cm³ at 298 K and 1 bar (experimental value 1.510 g/cm³). Similarly for [emim][B(CN)₄], the predicted density is 1.04 g/cm³ which is in good agreement with the experimental value 1.03 g/cm³ at 298 K and 1 bar.

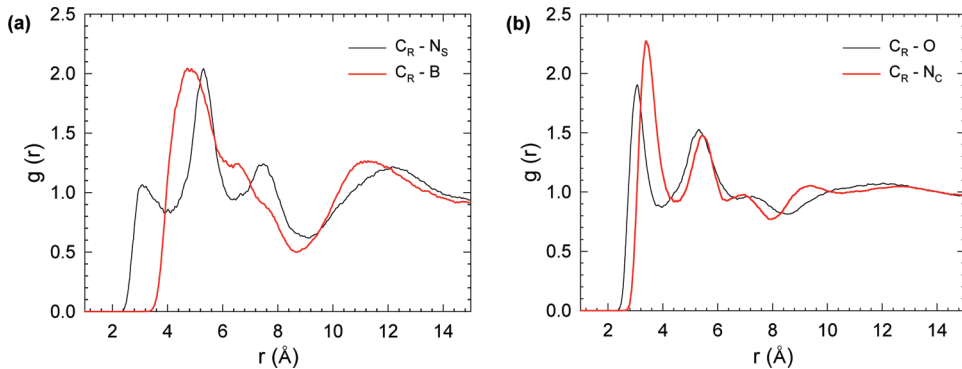


Figure 2. Atom–atom radial distribution functions between C_R atom of [emim] cation with (a) N_S of $[Tf_2N]$ and B of $[B(CN)_4]$ and (b) O of $[Tf_2N]$ and N_C of $[B(CN)_4]$. See Figure 1 for atom labels.

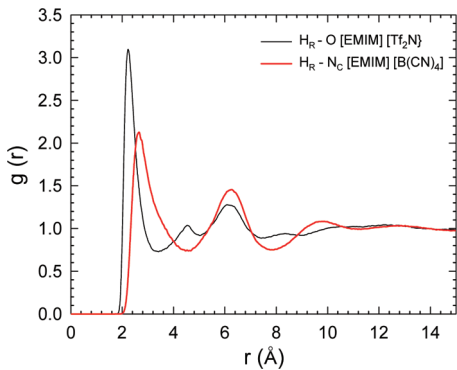


Figure 3. Atom–atom radial distribution functions between H_R atom of the [emim] cation with (a) O of $[Tf_2N]$ and (b) N_C of $[B(CN)_4]$. See Figure 1 for atom labels.

To understand the influence of anion on bulk liquid structure, structural correlations between cations and anions are analyzed from the trajectories obtained from the MD simulations at 298 K and 1 bar by comparing [emim][Tf_2N] and [emim][$B(CN)_4$]. Figure 2a shows the partial atom–atom radial distribution functions, $g(r)$, between the center atom of anion and C_R atom in the imidazolium ring of the cation. The C_R-N_S $g(r)$ of [emim]- $[Tf_2N]$ IL shows the first peak at ~ 3.25 Å and the second peak at ~ 5.4 Å. Similar structural correlation is observed between $[Tf_2N]$ anion with imidazolium-based cations that differ in the alkyl tail length.³⁴ However, in the case of [emim][$B(CN)_4$], the C_R-B $g(r)$ shows only a single peak at 4.8 Å which is much broader than those observed in [emim][Tf_2N]. Figure 2b shows the $g(r)$ between the most negatively charged atom in the anion and the C_R atom in the cation. Sharp peaks are observed in both ILs; the O atom of $[Tf_2N]$ anion is located closer to the C_R atom at a distance ~ 3.1 Å, compared to the N_C atom of $[B(CN)_4]$ which is located at ~ 3.4 Å. This indicates a weaker cohesion in the [emim][$B(CN)_4$] IL than in [emim][Tf_2N], which suggests that [emim][$B(CN)_4$] may be easier to expand than [emim][Tf_2N].

Further evidence of weaker cation–anion interaction in [emim][$B(CN)_4$] is reflected in the H-bonding. Figure 3 shows $g(r)$ between the H atom on the imidazolium ring (H_R) and O of $[Tf_2N]$ and N_C of $[B(CN)_4]$. The H_R-O $g(r)$ in [emim][Tf_2N] shows a strong peak at ~ 2.2 Å, typical of hydrogen bonding, while the H_R-N_C $g(r)$ in [emim][$B(CN)_4$] shows a peak at a greater distance (~ 2.7 Å) and 30% lower height. The H-bonding helps

the stronger cation–anion interaction found in [emim][Tf_2N], while in [emim][$B(CN)_4$] the strength of this H-bonding is dramatically reduced which again may help the [emim][$B(CN)_4$] IL to expand when CO_2 is dissolved.

3.2. Liquid Structure with CO_2 . Now we examine the solvation of CO_2 in [emim][Tf_2N] and [emim][$B(CN)_4$] from MD simulations. Several studies including experiments and molecular simulations have shown that the nature of anions has a profound effect on the interaction between CO_2 and ILs.^{11,19,35,36} Figure 4 shows the radial distribution functions between C atom in CO_2 and atoms in cations and anions for 0.2 mole fraction of CO_2 . As shown in Figure 4a, CO_2 is predominantly located near the O atom of $[Tf_2N]$ anion as evidenced by a short peak at ~ 3.3 Å. Similarly, from Figure 4b, we can see that the RDF between CO_2 and N_C atom of $[B(CN)_4]$ exhibits a strong peak at a distance of ~ 3.2 Å. In both ionic liquids, CO_2 is closer to the anion than to the cation as a result of the electrostatic attraction between the positively charged C atom of CO_2 and the negatively charged atoms on the anion. Comparing [emim][$B(CN)_4$] with [emim][Tf_2N], one can see that CO_2 interacts more strongly with $[B(CN)_4]^-$ than $[Tf_2N]^-$, as evidenced by the much sharper and higher first peak of CO_2 –anion interaction in the former. With the 12 Å cutoff radius, the coordination number of CO_2 around $[B(CN)_4]$ anions is computed to be 5.08, while it is 4.0 for $[Tf_2N]$, consistent with stronger coordination of CO_2 with $[B(CN)_4]$ anion.

To study the impact of CO_2 absorption on the liquid structure, partial radial distribution functions are plotted for cation–anion and anion–anion in the presence and absence of 0.2 mole fraction of CO_2 and shown in Figures S1 and S2 in the Supporting Information. No noticeable change is observed in both the cases, consistent with previous simulation studies which showed that even large amounts of CO_2 do not change much the underlying liquid structure of ILs.^{19,20,35}

3.3. Correlation between Interaction Energy and CO_2 Solubility. The classical MD simulations above show that the [emim][$B(CN)_4$] IL has a weaker cohesion than the [emim]- $[Tf_2N]$ IL but CO_2 interacts stronger with $[B(CN)_4]$ than with $[Tf_2N]$. This indicates two important factors affecting CO_2 solubility in ILs: (i) cation–anion interaction, and (ii) CO_2 –anion interaction. To determine which factor is dominating, we plotted the gas-phase cation–anion pair attraction against the measured CO_2 solubility for four ILs with the same cation (Figure 5). We found a good correlation between the cation–anion binding energy and CO_2 solubility (at 1 atm and room temperature), indicating that weaker cation–anion interaction is the dominant

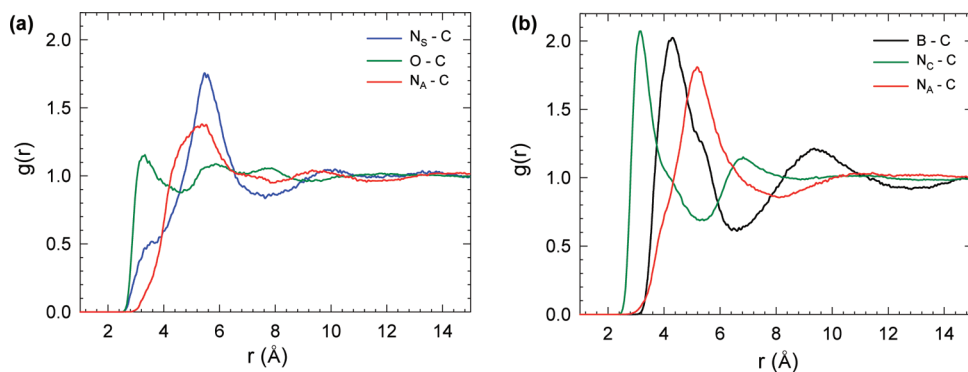


Figure 4. Atom–atom radial distribution functions between carbon atom in CO_2 and (a) N_s and O of $[\text{Tf}_2\text{N}]$ and N_A of $[\text{emim}]$ and (b) B and N_C of $[\text{B}(\text{CN})_4]$ and N_A atom of $[\text{emim}]$. See Figure 1 for atom labels.

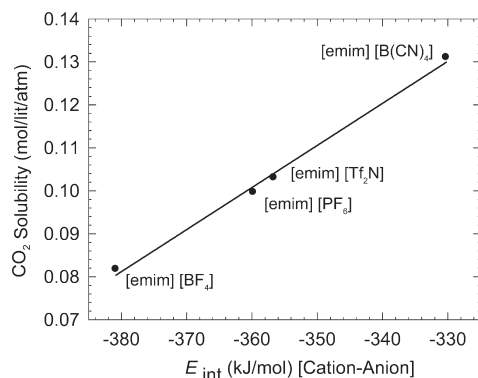


Figure 5. Correlation between gas-phase cation–anion interaction energy and the experimental CO_2 solubility at 1 bar and 298 K for four ionic liquids with the same 1-ethyl-3-methylimidazolium cation but different anions.^{2,6}

factor responsible for $[\text{emim}] [\text{B}(\text{CN})_4]$ ’s higher CO_2 solubility. This is reasonable in that, other things being equal, weaker cation–anion pair attraction allows easier expansion of the lattice and more CO_2 insertion into the interstitial space (or free volume).

The important role of the cation–anion interaction in affecting CO_2 solubility has also been discussed recently by others. For example, an ATR-IR experimental study showed that the solubility of CO_2 is greater in $[\text{bmim}] [\text{PF}_6^-]$ than in $[\text{bmim}] [\text{BF}_4^-]$ which can be attributed to larger swelling effect observed in the former due to weaker cation–anion interactions.³⁷ Kazarian et al. observed similar behavior and concluded that the binding energy of CO_2 –anion complex cannot be solely responsible for the high solubility of CO_2 in $[\text{bmim}] [\text{PF}_6^-]$ and a free volume contribution relating to weaker cation–anion interaction can play a dominant role.³⁸ This is also consistent with the ab initio calculations reported by Prasad et al.³⁹

To examine the effect of CO_2 –anion binding, we plotted the gas-phase CO_2 –anion interaction energy against the measured CO_2 solubility for four ILs with the same cation (Figure 6). One can see that the CO_2 –anion interaction energy does not correlate well with the CO_2 solubility, indicating that the CO_2 –anion attraction plays a secondary role for the high solubility of CO_2 in ILs. If one considers the Tf_2N anion as an outlier in Figure 6, it seems that the CO_2 solubility correlates with the gas-phase CO_2 –anion interaction. Similar behavior was also reported by others.⁴⁰ But this correlation is an inverse one and against physical intuition: it shows that weaker CO_2 –anion binding leads to greater CO_2

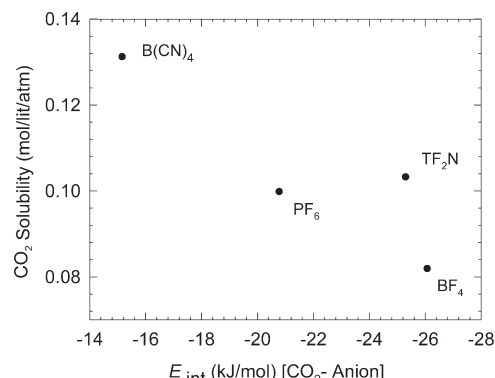


Figure 6. Correlation between the gas-phase CO_2 –anion interaction energy and the experimental CO_2 solubility at 1 bar and 298 K for four ionic liquids with the same 1-ethyl-3-methylimidazolium cation but different anions.^{2,6}

solubility for which we do not have a good explanation. We think that more data would be needed to establish a relationship between CO_2 solubility and the gas-phase CO_2 –anion interaction. In our case of the $\text{B}(\text{CN})_4$ anion, we think that the cation–anion interaction plays a more important role.

3.4. Volume Expansion. We have shown that the weak cation–anion interaction is primarily responsible for $[\text{emim}] [\text{B}(\text{CN})_4]$ ’s high CO_2 solubility. As a result of this weak interaction, the IL should experience more volume expansion during CO_2 absorption. To quantify this expansion, we calculated the percentage of volume expansion for both $[\text{emim}] [\text{Tf}_2\text{N}]$ and $[\text{emim}] [\text{B}(\text{CN})_4]$ ILs as a function of mole fraction of CO_2 at 298 K. The volume expansion is calculated as the difference of volume of mixture at a given temperature and pressure to the volume of pure liquid at the same temperature and ambient pressure. As shown in Figure 7, the percentage of volume expansion is indeed greater in $[\text{emim}] [\text{B}(\text{CN})_4]$ than in $[\text{emim}] [\text{Tf}_2\text{N}]$, consistent with the weaker cation–anion interaction in $[\text{emim}] [\text{B}(\text{CN})_4]$ which in turn results in more swelling with increasing mole fraction of CO_2 . Figure 8 shows the morphology of free volume in $[\text{emim}] [\text{B}(\text{CN})_4]$ at different mole fraction of CO_2 . The blue regions represent the void space. At low mole fraction, CO_2 tends to fill the small cavities present in the interior space and with increasing mole fraction, these small cavities group together to form large cavities with some interconnection. Similar behavior was observed by Huang et al.⁴¹

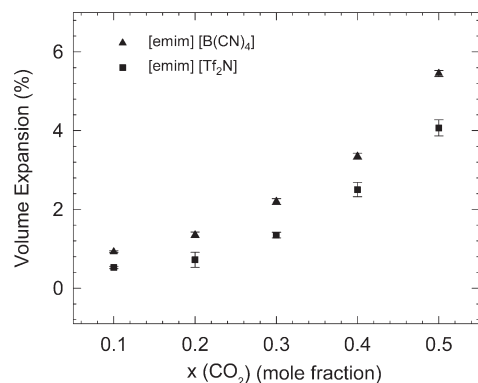


Figure 7. Volume expansion vs mole fraction for CO_2 in $[\text{emim}][\text{Tf}_2\text{N}]$ and $[\text{emim}][\text{B}(\text{CN})_4]$ at 298 K.

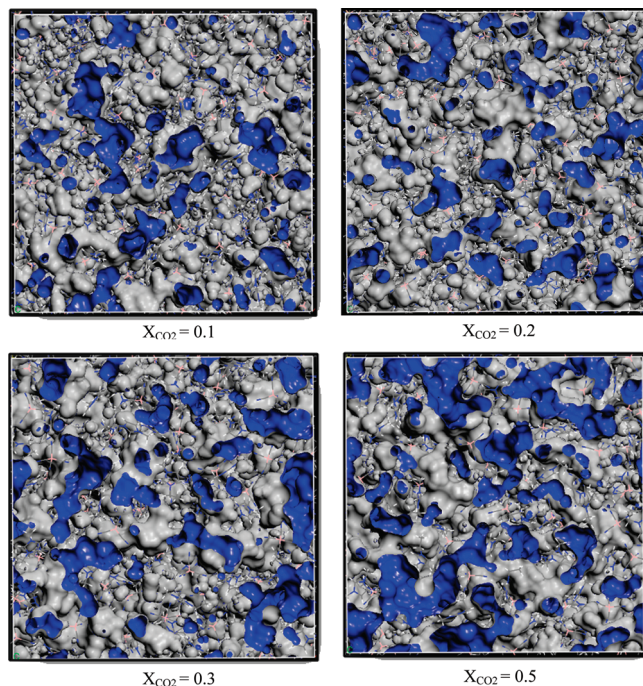


Figure 8. Morphology of free volume with varying mole fraction for CO_2 in $[\text{emim}][\text{B}(\text{CN})_4]$ at 298 K.

4. CONCLUSIONS

$[\text{emim}][\text{B}(\text{CN})_4]$ shows 30% higher CO_2 solubility than $[\text{emim}][\text{Tf}_2\text{N}]$ at 1.0 bar and 298 K. To study the underlying mechanism for the higher solubility of CO_2 in $[\text{emim}][\text{B}(\text{CN})_4]$ than in $[\text{emim}][\text{Tf}_2\text{N}]$, both $[\text{emim}][\text{B}(\text{CN})_4]-\text{CO}_2$ and $[\text{emim}][\text{Tf}_2\text{N}]-\text{CO}_2$ systems were analyzed using molecular dynamics simulation and quantum mechanical calculations. By analyzing the partial radial distribution functions (RDFs), it was found that the $[\text{B}(\text{CN})_4]$ anion is located slightly farther from $[\text{emim}]$ cation than is the $[\text{Tf}_2\text{N}]$ anion, indicating weaker structural correlation in $[\text{emim}][\text{B}(\text{CN})_4]$. This was found to be consistent with the weaker H-bonding in $[\text{emim}][\text{B}(\text{CN})_4]$. Stronger organization of CO_2 around the $[\text{B}(\text{CN})_4]$ anion was also found. A good correlation was observed between cation–anion interaction energy and CO_2 solubility at 1 bar. This suggested that weaker cation–anion interaction leads to higher CO_2 solubility

in $[\text{emim}][\text{B}(\text{CN})_4]$, consistent with a greater volume expansion observed in $[\text{emim}][\text{B}(\text{CN})_4]$ than in $[\text{emim}][\text{Tf}_2\text{N}]$.

■ ASSOCIATED CONTENT

S Supporting Information. Radial distribution functions (RDFs) in the presence and absence of CO_2 for $[\text{emim}][\text{Tf}_2\text{N}]$ and $[\text{emim}][\text{B}(\text{CN})_4]$, and RDFs between $[\text{emim}]$ and $[\text{BF}_4]$. This material is available free of charge via the Internet at <http://pubs.acs.org.org>.

■ AUTHOR INFORMATION

Corresponding Author

*E-mail: jiangd@ornl.gov.

■ ACKNOWLEDGMENT

This work was supported by the Division of Chemical Sciences, Geosciences, and Biosciences, Office of Basic Energy Sciences, U.S. Department of Energy. We thank Dr. Shannon Mahurin for helpful discussion and Dr. Oleg Borodin for giving us the force field parameter for $[\text{emim}][\text{B}(\text{CN})_4]$ ionic liquid. This research used resources of the National Energy Research Scientific Computing Center, which is supported by the Office of Science of the U.S. Department of Energy under Contract No. DE-AC02-05CH11231.

■ REFERENCES

- (1) Merkel, T. C.; Lin, H. Q.; Wei, X. T.; Baker, R. *J. Membr. Sci.* **2010**, *359*, 126.
- (2) Bara, J. E.; Carlisle, T. K.; Gabriel, C. J.; Camper, D.; Finotello, A.; Gin, D. L.; Noble, R. D. *Ind. Eng. Chem. Res.* **2009**, *48*, 2739.
- (3) Hu, Y. F.; Liu, Z. C.; Xu, C. M.; Zhang, X. M. *Chem. Soc. Rev.* **2011**, *40*, 3802.
- (4) Keskin, S.; Kayrak-Talay, D.; Akman, U.; Hortacsu, O. *J. Supercrit. Fluids* **2007**, *43*, 150.
- (5) Noble, R. D.; Gin, D. L. *J. Membr. Sci.* **2011**, *369*, 1.
- (6) Mahurin, S. M.; Lee, J. S.; Baker, G. A.; Luo, H. M.; Dai, S. *J. Membr. Sci.* **2010**, *353*, 177.
- (7) Aki, S.; Mellein, B. R.; Saurer, E. M.; Brennecke, J. F. *J. Phys. Chem. B* **2004**, *108*, 20355.
- (8) Camper, D.; Bara, J.; Koval, C.; Noble, R. *Ind. Eng. Chem. Res.* **2006**, *45*, 6279.
- (9) Camper, D.; Scovazzo, P.; Koval, C.; Noble, R. *Ind. Eng. Chem. Res.* **2004**, *43*, 3049.
- (10) Carlisle, T. K.; Bara, J. E.; Gabriel, C. J.; Noble, R. D.; Gin, D. L. *Ind. Eng. Chem. Res.* **2008**, *47*, 7005.
- (11) Muldoon, M. J.; Aki, S.; Anderson, J. L.; Dixon, J. K.; Brennecke, J. F. *J. Phys. Chem. B* **2007**, *111*, 9001.
- (12) Bara, J. E.; Gabriel, C. J.; Lessmann, S.; Carlisle, T. K.; Finotello, A.; Gin, D. L.; Noble, R. D. *Ind. Eng. Chem. Res.* **2007**, *46*, 5380.
- (13) Moganty, S. S.; Baltus, R. E. *Ind. Eng. Chem. Res.* **2010**, *49*, 9370.
- (14) Vega, L. F.; Vilaseca, O.; Llorell, F.; Andreu, J. S. *Fluid Phase Equilib.* **2010**, *294*, 15.
- (15) Diedenhofen, M.; Klamt, A. *Fluid Phase Equilib.* **2010**, *294*, 31.
- (16) Palomar, J.; Gonzalez-Miquel, M.; Polo, A.; Rodriguez, F. *Ind. Eng. Chem. Res.* **2011**, *50*, 3452.
- (17) Bhargava, B. L.; Balasubramanian, S. *J. Chem. Phys.* **2007**, *127*, 114510.
- (18) Bhargava, B. L.; Balasubramanian, S. *J. Phys. Chem. B* **2007**, *111*, 4477.
- (19) Shi, W.; Maginn, E. J. *J. Phys. Chem. B* **2008**, *112*, 2045.
- (20) Zhang, X. C.; Huo, F.; Liu, Z. P.; Wang, W. C.; Shi, W.; Maginn, E. J. *J. Phys. Chem. B* **2009**, *113*, 7591.

- (21) Kirchner, B. *Ionic Liquids*; Springer: New York, 2009; Topics in Current Chemistry Vol. 290, p 213.
- (22) Maginn, E. J. *J. Phys. Condens. Matter* **2009**, *21*, 373101.
- (23) Borodin, O. *J. Phys. Chem. B* **2009**, *113*, 11463.
- (24) Bedrov, D.; Borodin, O.; Li, Z.; Smith, G. D. *J. Phys. Chem. B* **2010**, *114*, 4984.
- (25) Yan, T. Y.; Wang, Y. T.; Knox, C. *J. Phys. Chem. B* **2010**, *114*, 6886.
- (26) Yan, T. Y.; Wang, Y. T.; Knox, C. *J. Phys. Chem. B* **2010**, *114*, 6905.
- (27) Smith, W.; Forester, T. R. *J. Mol. Graph.* **1996**, *14*, 136.
- (28) Koddermann, T.; Paschek, D.; Ludwig, R. *Chemphyschem* **2007**, *8*, 2464.
- (29) Liu, Z. P.; Huang, S. P.; Wang, W. C. *J. Phys. Chem. B* **2004**, *108*, 12978.
- (30) Harris, J. G.; Yung, K. H. *J. Phys. Chem.* **1995**, *99*, 12021.
- (31) Martinez, L.; Andrade, R.; Birgin, E. G.; Martinez, J. M. *J. Comput. Chem.* **2009**, *30*, 2157.
- (32) Ahlrichs, R.; Bar, M.; Haser, M.; Horn, H.; Kolmel, C. *Chem. Phys. Lett.* **1989**, *162*, 165.
- (33) Koddermann, T.; Paschek, D.; Ludwig, R. *Chemphyschem* **2008**, *9*, 549.
- (34) Logothetis, G. E.; Ramos, J.; Economou, I. G. *J. Phys. Chem. B* **2009**, *113*, 7211.
- (35) Cadena, C.; Anthony, J. L.; Shah, J. K.; Morrow, T. I.; Brennecke, J. F.; Maginn, E. J. *J. Am. Chem. Soc.* **2004**, *126*, 5300.
- (36) Bhargava, B. L.; Krishna, A. C.; Balasubramanian, S. *AIChE J.* **2008**, *54*, 2971.
- (37) Lim, B. H.; Choe, W. H.; Shim, J. J.; Ra, C. S.; Tuma, D.; Lee, H.; Lee, C. S. *Korean J. Chem. Eng.* **2009**, *26*, 1130.
- (38) Kazarian, S. G.; Briscoe, B. J.; Welton, T. *Chem. Commun.* **2000**, 2047.
- (39) Prasad, B. R.; Senapati, S. *J. Phys. Chem. B* **2009**, *113*, 4739.
- (40) Bhargava, B. L.; Balasubramanian, S. *Chem. Phys. Lett.* **2007**, *444*, 242.
- (41) Huang, X. H.; Margulis, C. J.; Li, Y. H.; Berne, B. J. *J. Am. Chem. Soc.* **2005**, *127*, 17842.